Geophys. J. Int. (2002) **148,** 340–347

RESEARCH NOTE

Predictions of secular geoid changes from Late Pleistocene and Holocene Antarctic ice-ocean mass imbalance

Georg Kaufmann

Institute of Geophysics, University of Göttingen, Herzberger Landstrasse 180, 37075 *Göttingen, Germany. E-mail: gkaufmann@uni-geophys.gwdg.de*

Accepted 2001 September 3. Received 2001 August 30; in original form 2001 May 4

SUMMARY

Estimates on ice volume changes in Antarctica, from both contemporary mass imbalance during the last hundred to thousand years and ice volume changes during the last glacial cycles, are difficult to obtain. Future satellite-gravity missions monitoring secular changes in gravity as a proxy of mass changes of the Antarctic Ice Sheet will therefore provide an additional important constraint on the Antarctic Ice Sheet history. We assess the contributions from both past ice volume changes during the last glacial cycles and present ice imbalances over Antarctica, using a variety of published ice models. Model predictions of secular changes of the geoid anomaly based on plausible mantle viscosity profiles enable us to discuss the importance of past and present ice volume changes and their characteristic signatures. While uncertainties arising from the viscosity profile are of secondary importance for model predictions of the secular change of the geoid anomaly, we expect significant bias of the observed signal from uncertainties in the timing of the end of deglaciation, which is in agreement with previous studies. Hence, the benefit of inferring present-day Antarctic ice imbalance from satellite-gravity missions will depend on improvements to ice models for the last glacial cycle.

Key words: Antarctic Ice Sheet, geoid anomalies, last glacial cycles, present-day melting.

1 INTRODUCTION

The reconstruction of the evolution of the Antarctic Ice Sheet throughout the last glacial cycles is inconclusive. Indirect observations such as successions of ancient beaches recording relative sea-level changes are rare in Antarctica, a consequence of the small number of localities of exposed bedrock. Observations on the variability of the climate throughout the last glacial cycles used to reconstruct the Antarctic Ice Sheet by climate-controlled modelling of ice sheet dynamics (e.g. Huybrechts 1990) provide another means to investigate fluctuations in the Antarctic ice volume.

1.1 Space-geodetic measurements

Improvements in measuring geodetic signatures reflecting the isostatic response to fluctuations in ice volume are particularly useful to constrain further the evolution of the Antarctic Ice Sheet. Here, continuous Global Positioning System (GPS) monitoring of the present-day motions has been proposed as a means of ice sheet reconstructions (e.g. James & Ivins 1995; Wahr *et al.* 1995; James & Ivins 1997, 1998; Zwartz *et al.* 1999). Surface-gravity measurements have also been proposed (e.g. Wahr *et al.* 1995; James & Ivins 1998) as an addition to GPS campaigns further constraining ice volume changes. Also, the significance of secular changes in the geoid anomaly caused by past and present ice volume changes as a constraint for ice sheet reconstructions has been appreciated recently (e.g. Bentley & Wahr 1998).

Measurements of the Earth's gravitational field and its secular variations will be improved significantly by satellite-gravity missions such as CHAMP and GRACE within the next decade. For the gravitational field and its temporal variation surveyed by CHAMP, the accuracy of the long-wavelength signal will be improved by one order of magnitude, and the geoidal surface will be determined to within the centimetre level (Reigber *et al.* 1996). The high signal-to-noise ratio of the temporal variations in the gravitational field allows separation of different sources of the orbital perturbations such as atmospheric mass redistributions, ocean circulation, contemporary sea-level changes and mass changes within the Earth. The GRACE mission will extend and complement the CHAMP mission, with the additional potential to resolve the time-dependent gravitational field by another order of magnitude.

The satellite-gravity missions have several advantages and disadvantages for inferences of ice volume changes. According to Bentley & Wahr (1998), the gravity signal as an integral measure of mass changes provides a convenient way to assess spatial variability of ice imbalance over Antarctica, especially in areas which are beyond the reach of expeditions. However, secular changes in the geoid anomaly are a result of several effects, for example (i) present-day mass imbalance, (ii) past ice volume changes during the last glacial cycles, (iii) interannual variations in snow balance and (iv) interannual variations in mean atmospheric pressure. An assessment of the above effects on the observations of a satellite-gravity mission has been given in Bentley & Wahr (1998).

1.2 Previous work

A number of studies have been performed on predicting the response of the Earth to changes in the Antarctic Ice Sheet. For example, James & Ivins (1997) have developed four scenarios of present-day ice mass imbalances over Antarctica from an extensive review of the available literature. The scenarios developed provide vastly different rates for secular sea-level change, ranging from -1.1 to 0.45 mm yr^{-1}. The authors argue that a well-constrained set of observations for the low-degree Stokes coefficients can be used to constrain both the present-day ice mass imbalance and the radial mantle viscosity profile. In James & Ivins (1998), the authors predict crustal responses in Antarctica from both present-day mass imbalance models and deglaciation models of the last ice-age cycle. The predictions are based on solutions of the sea-level equation with a eustatic ocean loading term. Two contributions are discussed, the elastic response due to present-day mass imbalance and the viscoelastic response resulting from variations in ice heights during the last glacial cycle. For the former models, the present-day scenarios of James & Ivins (1997) have been used, and vertical rates of crustal movement are generally below 5 mm yr^{-1}, with local uplift above 5–10 mm yr^{-1} focused on areas such as the Riiser–Larsen and Ronne–Filcher ice shelves, and local subsidence below 4–5 mm yr^{-1} around the Pine Island glacier. The ice models for the last glacial cycle are either derivatives of the CLIMAP model of Denton & Hughes (1981), such as the LC79, ICE-3G and ICE-4G models, or a more recent revision such as the D91 model of Denton *et al.* (1991). In general, the postglacial signal of crustal uplift for the CLIMAP-based models is larger than for the present-day scenarios, with uplift above 10 mm yr^{-1} over West Antarctica and less than 5 mm yr^{-1} over East Antarctica. Peak values are around 20–25 mm yr^{-1} over the Ross and Ronne–Filchner ice shelves and the Antarctic Peninsula. The D91 model results in less uplift, as the ice mass loss during the last deglaciation has been substantially reduced. Nonetheless, areas such as the Antarctic Peninsula and the Ross Ice Shelf are predicted to rise by about 8–15 mm yr^{-1}. Dependence of the crustal movement on mantle viscosity has been shown to be of secondary importance. However, the timing of deglaciation has been shown to be a key parameter controlling the crustal motion signal. Zwartz *et al.* (1999) have proposed a GPS campaign along the Lambert Glacier, a large glacier draining about 10 per cent of the East Antarctic Ice Sheet towards the Amery Ice Shelf. The authors argue that the expected accuracy of a repeated GPS campaign, especially the measured vertical motion, can be useful in discriminating between different deglaciation scenarios of the Antarctic Ice Sheet. Again, it is expected to be able to constrain the timing of deglaciation better.

1.3 Objectives

In this paper, we discuss model predictions for secular variations in the geoid resulting from past and present-day ice volume changes in Antarctica in view of the expected improvements in observed geoid and gravity anomalies from the satellite-gravity missions. We employ three Antarctic ice models for the Late Pleistocene ice–ocean mass imbalance, and three recently proposed scenarios for the present-day Antarctic ice imbalance. We extent the present-day melting scenarios back in time to simulate recent mass changes, hence a viscoelastic component is added to the recent ice–ocean mass imbalance. We also solve the sea-level equation in a more consistent way as done in the previous work of James & Ivins (1998), as we take into account all major Pleistocene ice sheets and redistribute the meltwater in a physically consistent way. For the viscoelastic response of the Earth to ice mass changes we use a recent mantle viscosity profile derived from a formal inversion of glacial isostatic adjustment observations (Kaufmann & Lambeck 2002), which also satisfies the long-wavelength geoid constraint for mantle circulation modelling. Hence, we improve the James & Ivins (1998) work by using more recent models of past ice models (e.g. Huybrechts 1990) and of the radial mantle viscosity profile (e.g. Kaufmann & Lambeck 2002), and a physically consistent solution of the sea-level equation on a rotating earth.

2 EARTH MODELS

The earth model is defined as a spherically symmetric, compressible, Maxwell-viscoelastic continuum. The elastic structure is based on PREM (Dziewonski & Anderson 1981), and the radial viscosity profile is taken as a variable parameter. An elastic lithosphere is modelled as a top layer with infinite viscosity and a sublithospheric viscoelastic mantle subdivided into layers of constant viscosity. The earth's core is represented as inviscid fluid and incorporated as a lower boundary condition. The viscosity model used is based on an analysis of various signatures related to the glacial isostatic adjustment process (ancient beach sequences, present-day uplift rates, changes in the Earth's rotation and gravity field) performed by Kaufmann & Lambeck (2002). In this paper, a formal inverse procedure has been used to fit the observations. The resulting viscosity profile shown in Fig. 1 is characterized by an elastic lithosphere of around 100 km thickness, and a sublithospheric viscosity increasing from 2×10^{20} Pa s below the lithosphere to almost 10^{23} Pa s at mid-mantle depths (1000–1200 km), then decreasing again. Viscosity in this model varies rather smoothly, and no significant jump in viscosity across the 660 km seismic discontinuity is present. This viscosity profile is also able to provide a good fit to the long-wavelength geoid constraint for mantle circulation models (Kaufmann & Lambeck 2000). For comparison purposes, we have derived a three-layer volume-averaged viscosity profile with viscosities in the upper and lower mantle of 9.7×10^{20} and 1.8×10^{22} Pa s, respectively (dashed line in Fig. 1).

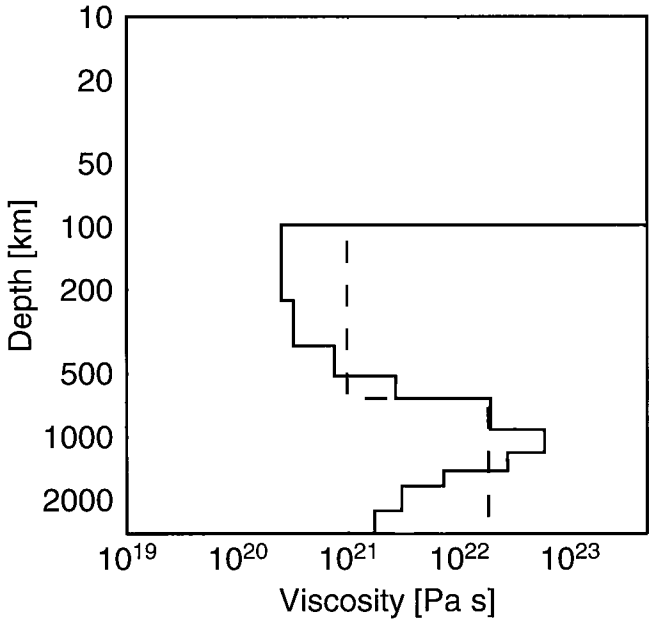

Figure 1. Multilayer (solid line) and volume-averaged three-layer (dashed line) viscosity profiles (from Kaufmann & Lambeck 2002).

3 ICE MODELS

We have based our model predictions on three Late Pleistocene models for the Antarctic Ice Sheet (Figs 2a–c), which we term past ice models. These past ice models are chosen to encompass a wide range of plausible scenarios, in terms of both the total amount of meltwater discharged and the timing of the last deglaciation phase. However, we make no attempt to favour a particular ice model as the most realistic one, as the uncertainty of the last glacial cycle in Antarctica is still too large.

Model ANT3 (Nakada & Lambeck 1988) is based on the CLIMAP reconstruction. It is derived as the difference between the last glacial maximum (LGM) Antarctic model from Denton & Hughes (1981) and the present-day Antarctic Ice Sheet of Drewry (1982). Model ANT3 contributes 37 m of eustatic sea-level (ESL) rise since the LGM. The main deglaciation in this model was rather early, with ANT3 melting between 17 and 6.4 kyr BP. At the LGM, the model is characterized by three large ice domes, the largest one over the Ronne–Filchner Ice Shelf, and smaller ones over the Ross Ice Shelf and the Antarctic Peninsula, and significant additional ice over the coastal regions in East Antarctica. Model ICE-3G is the Antarctic Ice Sheet reconstruction from the global ice model ICE-3G (Tushingham & Peltier 1991); it is also based on the CLIMAP reconstruction. The ESL contribution of ICE-3G is 25 m, but the timing of the deglaciation, mainly from 10–4 kyr BP, favours a late disintegration of the Antarctic Ice Sheet. The disintegration period has been chosen to match sea-level observations in the far field, in this case the Wairau Valley site in New Zealand. At the LGM, this model has the largest ice dome over the Ross Ice Shelf, and two smaller domes over the Ronne-Filchner Ice Shelf and the Antarctic Peninsula. Model HUY from Huybrechts (1990) is derived from thermomechanical modelling of the ice flow; it contributes only 13 m to ESL. The timing of the deglaciation is in contrast to the two geomorphological models, with melting occurring mostly after 6.4 kyr BP and continuing until the present. Between the LGM and around 10 kyr BP, the model exhibits ice domes over the Ronne–Filchner and Ross Ice Shelves, and almost no additional ice over East Antarctica, except a small ice dome.

All three Antarctic ice models are supplemented by the northern hemisphere ice models ICE-1 (Peltier & Andrews 1976) for the Laurentide Ice Sheet and Greenland, model FBKS8 (Lambeck *et al.* 1998a) for the Fennoscandian and Barents Sea ice sheets, and model BK4 (Lambeck 1993) for the British Ice Sheet. We simulate the Late Pleistocene glacial cycles by modelling the last two cycles in accordance with the $\delta^{18}O$ record (Chappell & Shackleton 1986), and by assuming an average ice load before that time. This parametrization of the last glacial cycles has been shown to be sufficient to predict correctly changes in the Earth's gravitational field and rotation (Johnston & Lambeck 1999). Times in this context are given in calendar years.

In addition to the Late Pleistocene melting we study the present S1, S2M and J92 scenarios (Fig. 2d–f) for the recent mass imbalance of the Antarctic Ice Sheet (James & Ivins 1997) to account for the effects of contemporary melting on geodetic signatures as the secular change in geoid. The S1 scenario is derived from mass imbalance observations of Antarctic drainage basins and represents a minimalistic model, with the present-day Antarctic Ice Sheet generally in balance except a growing Pine Island Glacier and a shrinking Riiser–Larsen Ice Shelf. Scenario S2M has been derived from extrapolations of mass imbalances of the drainage basins from measured to unmeasured regions, and imbalances occur mainly along the Antarctic coastline, where ice sheets are growing. Both S1 and S2M have a positive mass imbalance and thus contribute to a falling global ESL by about -0.1 and -1.1 mm yr^{-1}, respectively. In contrast, J92 has a negative mass imbalance, with a global ESL rise of about 0.45 mm yr^{-1}. In this scenario, mass imbalances are mainly occurring inland of the Filchner–Ronne and Ross Ice Shelves. Thus, J92 provides half of the observed present-day sea-level rise of around 1 mm yr^{-1} (Gornitz *et al.* 1982; Lambeck *et al.* 1998b). In contrast to recent modelling of the elastic response to contemporary Antarctic mass imbalance in James & Ivins (1998), we allow a contemporary imbalance for 100 years to reflect uncertainties in the timing of present-day meltwater contributions. Hence, we assume that the recent mass changes can be extrapolated backwards in time.

4 RESULTS

We solve the sea-level equation on a rotating earth using the pseudospectral approach (Mitrovica & Peltier 1991; Milne & Mitrovica 1998). Spherical harmonic expansions are truncated at $l=192$.

4.1 Past and present ice models

We start by discussing model predictions for the secular variation of the geoid anomaly, $\dot{g}$, for the three Late Pleistocene ice models ANT3, ICE-3G, and HUY (Fig. 3a–c). Model predictions for ANT3 reflect the early disappearance of the additional ice by about 6400 yr, with peak amplitudes around $\dot{g} \simeq 1.5$ mm yr^{-1} over the Ronne–Filchner Ice Shelf, the main LGM ice dome in ANT3. Values above 1 mm yr^{-1} are predicted also above the grounding line of the Ross Ice Shelf, but over East Antarctica $\dot{g}$ is generally below 0.5 mm yr^{-1}.

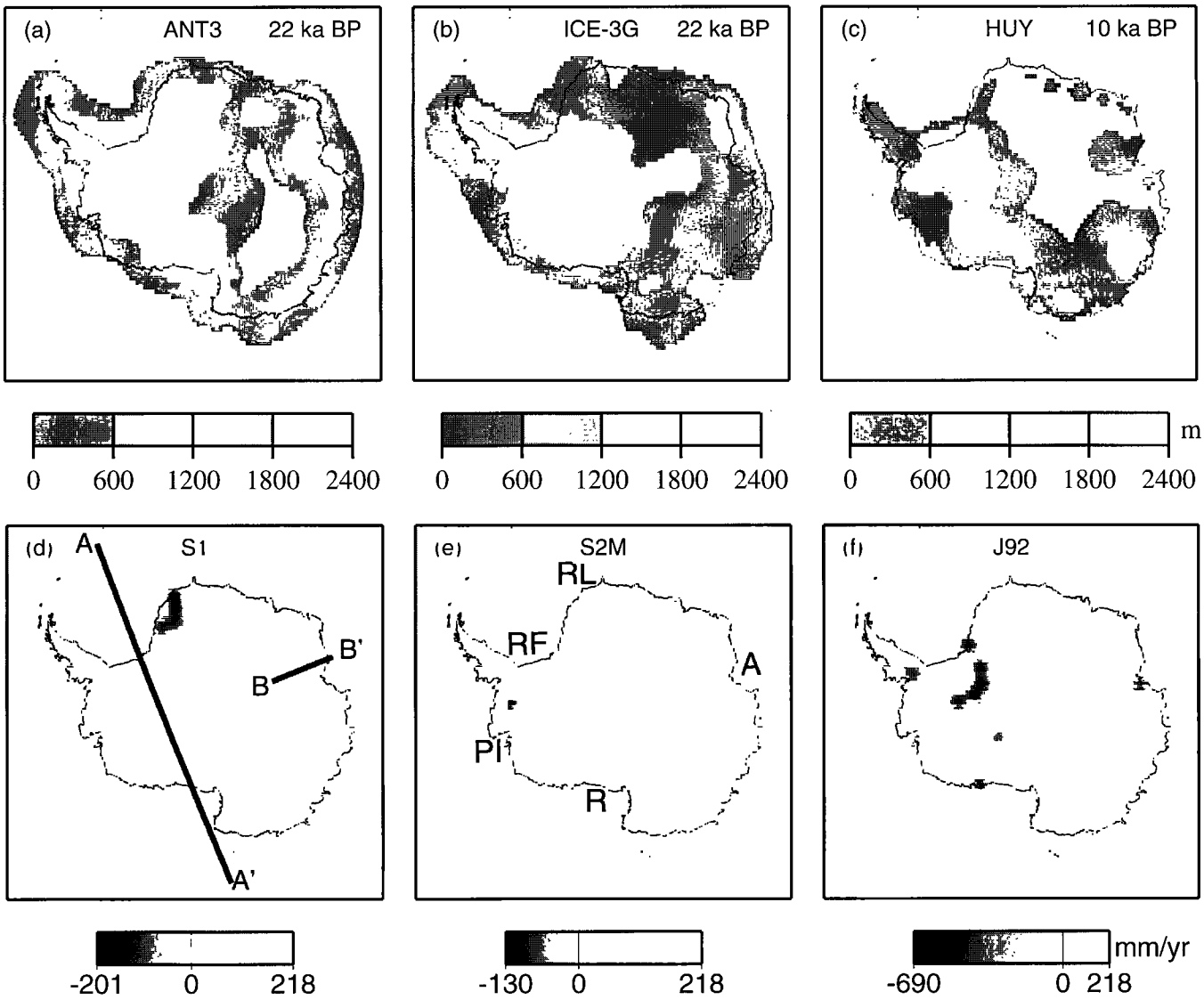

Figure 2. Maximum extent of different Late Pleistocene Antarctic ice models ANT3, ICE-3G and HUY (a–c) and contemporary melting scenarios S1, S2M and J92 (d–f). Note that model HUY has reached its maximum extent at 10 000 yr BP. The two profiles A–A′ and B–B′ shown in (d) are used later. The bold letters in (e) indicate the position of Ronne–Filchner Ice Shelf (RF), Riiser–Larsen Ice Shelf (RL), Ross Ice Shelf (R), Amery Ice Shelf (A), and Pine Island Glacier (PI).

Predictions for ICE-3G result in larger rates for $\dot{g}$, with peak amplitudes around 2 mm yr^{-1} over the Ross Ice Shelf, which is the location of the most prominent LGM ice dome in this model. As expected, the late disappearance of the Ross Ice Dome around 4000 yr BP is reflected in larger values of $\dot{g}$, because the remaining isostatic disequilibrium is much larger than for the ANT3 predictions. Values above 1 mm yr^{-1} are predicted over the whole of West Antarctica and large parts of East Antarctica, and the 0.5 mm yr^{-1} contour encompasses the entire continent. Predictions for HUY are even larger, with maxima around 3 and 1.5 mm yr^{-1} located over the two ice domes of this model, the larger Ronne–Filchner Ice Dome and the smaller East Antarctic Ice Dome. The large predictions of $\dot{g}$ reflect the recent mass changes in HUY during the Holocene period, with significant ice volume changes until the present. Despite predictions of $\dot{g}$ above 0.5 mm yr^{-1} for the entire continent, the main difference with respect to the two geomorphological models is the peak over East Antarctica.

For the three contemporary ice models S1, S2M and J92 shown in Figs 3(d)–(f), predictions of $\dot{g}$ closely reflect the mass imbalances of the models. For S1, a minimalistic scenario featuring a balanced present-day Antarctic Ice Sheet except a growing Pine Island Glacier and a shrinking Riiser–Larsen Ice Shelf, significant changes of $\dot{g}$ below -1 mm yr^{-1} are only predicted over the Pine Island Glacier. Values above 1 mm yr^{-1} are focused around the Riiser–Larsen Ice Shelf. For S2M, positive mass imbalances are mainly focused around the Antarctic coastal margin. Consequently, significant predictions of $\dot{g}$ below -1.5 mm yr^{-1} are restricted to coastal areas, with the exception of the Pine Island Glacier. In J92, the only scenario with a negative mass imbalance, significant melting occurs around the grounding lines of the Ronne–Filchner, Ross and Amery ice shelves. Again, the Pine Island Glacier is assumed to grow. These mass imbalance patterns are reflected in predictions of $\dot{g}$, with large values above 3 mm yr^{-1} along the grounding lines of the large ice shelves, and a decrease of

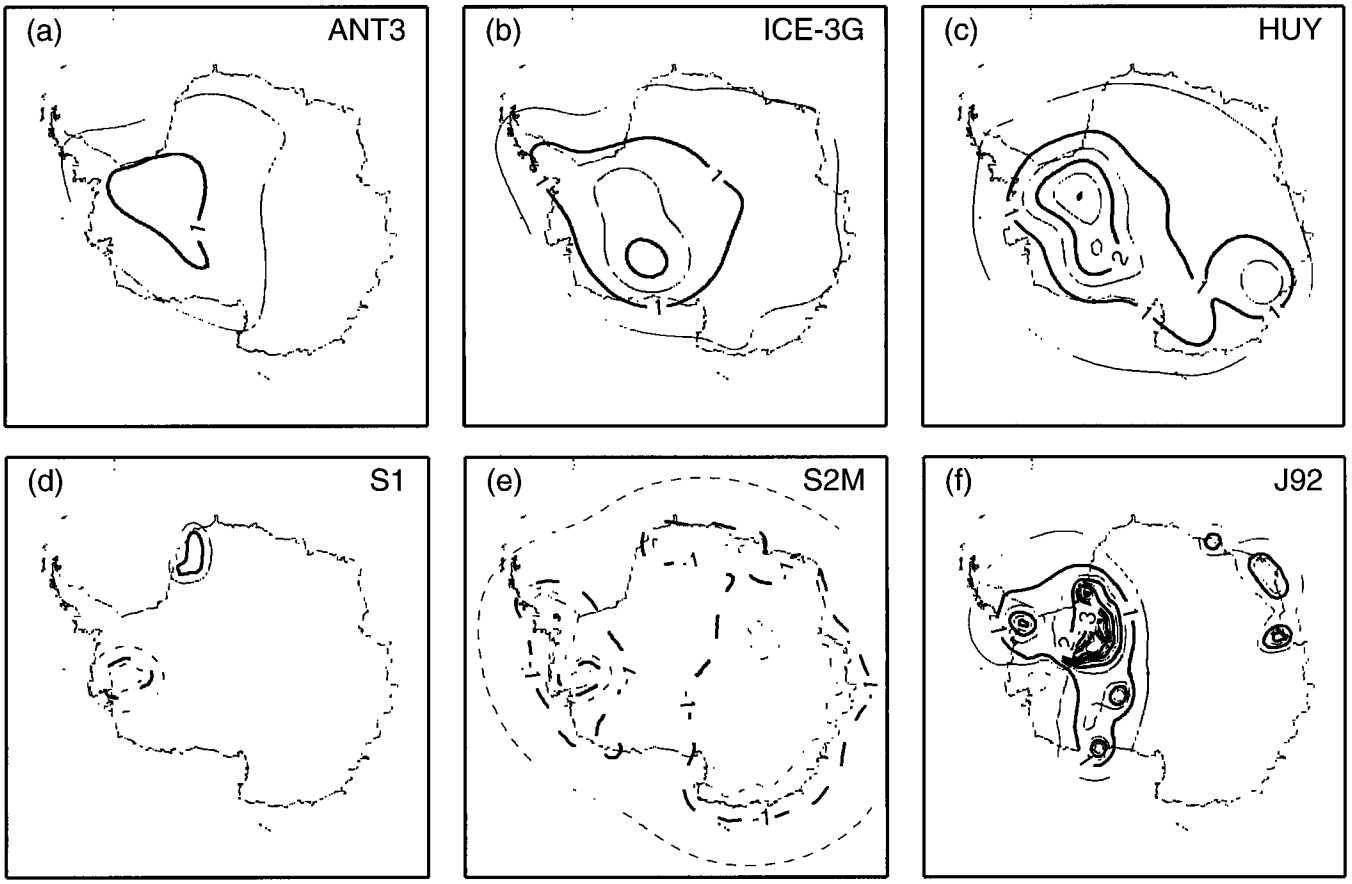

Figure 3. Predictions of secular variations in geoid anomaly (in mm yr^{-1}) for the three different Late Pleistocene ice models ANT3, ICE-3G and HUY (a–c) and three contemporary melting scenarios S1, S2M and (d–f). Contours are drawn every 0.5 mm yr^{-1} (solid lines for positive, dashed lines for negative values), and the zero contour is omitted.

0.5 mm yr^{-1} over the Pine Island Glacier. For all present-day mass imbalance scenarios, the predicted response to changes in geoid anomaly is fairly localized, while the predicted signal resulting from the disintegration of the past ice sheets is broader. We note that our predictions of $\dot{g}$ for S1, S2M and J92 closely match the patterns for predictions of secular variations in solid-surface gravity anomalies presented in James & Ivins (1998), which we take as a proof of the accuracy of our numerical resolution.

In Fig. 4, the power spectra of the secular variations in the geoid anomaly are shown for the different ice models. The power spectra are fully normalized and are equivalent to the degree variances often used in geodetic applications. The two lines shown are estimates of the expected resolution of the GRACE satellite-gravity mission, derived for 1 yr and a 5 yr observational periods. For all past ice models, the spectra decrease around two to three orders of magnitude from Legendre degree two up to 50. However, the main deglaciation phase of the past ice models determines the decrease in amplitude, with amplitudes for model ANT3 dropping faster than for model HUY. Model ICE-3G is in between the two responses. Hence, ice models favouring an early deglaciation phase will lose short-scale information, and the predicted signal drops below the expected observational uncertainty for Legendre degrees larger than 25.

For the three present-day mass imbalance models, the predicted power spectra are more uniform. The amplitudes for all models are above the observational uncertainties up to Legendre degrees of 40 to 45. Hence, the decrease in amplitude is less pronounced than for the past ice models. In fact, if we combine the past and present ice model responses, the contributions from present-day mass imbalance models dominate the spectral response for Legendre degrees above 25.

4.2 Profile predictions

In Fig. 5, we have summarized predictions of $\dot{g}$ along two profiles. The profile locations are redrawn in Fig. 2(d), with profile A–A′ crossing the Ronne–Filchner and Ross ice shelves, thus sampling the regions of both major LGM ice domes and areas of significant contemporary melting. Profile B–B′ is a transect along the site of the Lambert Glacier, which calves into the Amery Ice Shelf. The latter profile has been chosen by Zwartz *et al.* (1999) for predictions of the vertical uplift rate for the same three ice models of the last glacial cycle. We demonstrate two points in Fig. 5, the dependence of the predictions of $\dot{g}$ on the radial viscosity profile, and the influence of contemporary melting on predictions of $\dot{g}$.

In Fig. 5(a), predictions of $\dot{g}$ along profile A–A′ are shown for ice models ANT3, ICE-3G and HUY. For each ice model, the predictions shown are derived from two different viscosity profiles, the multilayer profile shown as a solid line in Fig. 1 and a corresponding volume-averaged three-layer viscosity profile

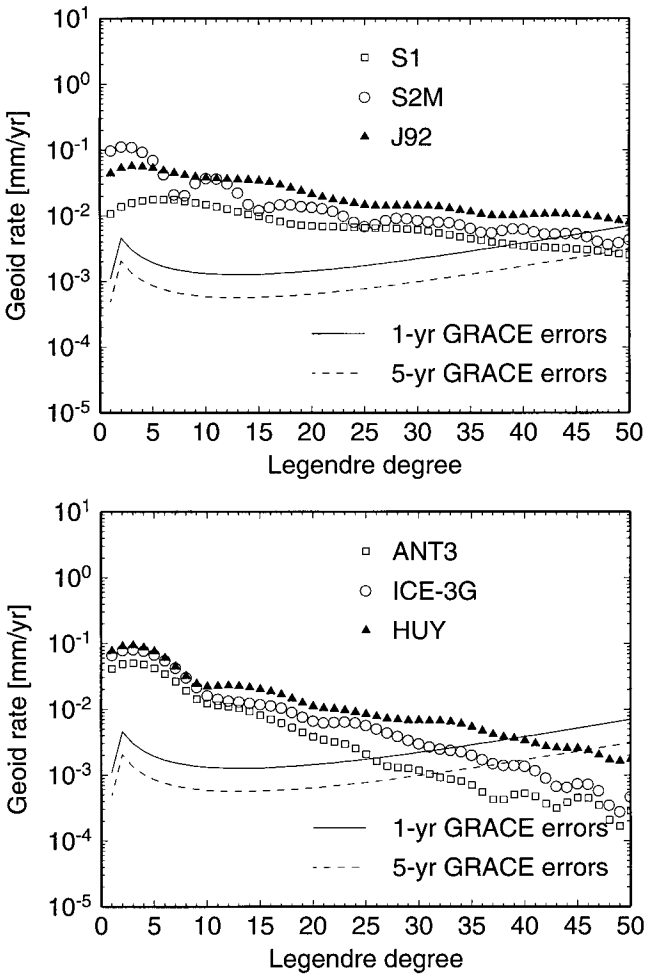

Figure 4. Power spectra of secular variations in geoid anomaly (in mm yr^{-1}) for the three different Late Pleistocene ice models ANT3, ICE-3G, and HUY (top) and three contemporary melting scenarios S1, S2M and J92 (bottom). Lines indicate the expected resolution of the GRACE satellite-gravity mission.

shown as a dashed line in Fig. 1. These two viscosity profiles are chosen to answer the question how sensitive the secular rate of geoid anomalies is to details in the vertical viscosity stratification. As expected, predictions for ice model HUY are largest and those for ice model ANT3 are smallest, reflecting the different assumptions on the deglaciation phases of the ice models. Peak amplitudes are around 1, 2 and 3 mm yr^{-1} for ANT3, ICE-3G and HUY, respectively. Within the range of viscosity profiles considered, the variability of $\dot{g}$ in the 1σ uncertainty is always less than ± 0.2 mm yr^{-1}. Thus uncertainties arising from a more detailed viscosity stratification can be regarded as being of secondary importance for predictions of $\dot{g}$. This conclusion is in line with earlier inferences of the importance of the viscosity structure on predictions of geodetic parameters such as present-day motions (e.g. James & Ivins 1998).

Next, we discuss predictions of $\dot{g}$ for the three models ANT3, ICE-3G and HUY combined with the contemporary melting scenario J92, which we have chosen as an upper bound to illustrate the effect of present-day melting. For predictions of $\dot{g}$ along profile A-A′ shown in Fig. 5(b), we obtain a dominant signal from the contemporary melting model located over the grounding lines of the Ronne–Filchner and Ross Ice Shelves, visible in two large peaks. Variability arising from different viscosity profiles is again of secondary importance. Peak amplitudes of the combined past and present ice models are at least twice as large as for the LGM ice models alone and exhibit the short-scale variability of the contemporary melting mentioned earlier.

In Fig. 5(c), predictions of $\dot{g}$ along profile B–B′ are shown for the set of past ice models and the two viscosity profiles. The shape of the model predictions varies smoothly along the profile, decreasing towards the coast and not exceeding 1 mm yr^{-1}. Uncertainties from the more detailed viscosity stratification are again small, with variations of up to 0.2 mm yr^{-1}. If we add the contemporary ice imbalance model J92 as done in Fig. 5(d), the predicted change in geoid anomaly becomes larger over the downstream end of the Lambert Glacier, but smaller further up the glacier. Clearly, the enhanced signal is attributable to the J92 scenario.

5 CONCLUSIONS

We conclude that both the past and present ice volume changes over Antarctica simulated in this paper have a significant effect on secular changes in the geoid anomaly, which in turn has the potential to be resolved by future satellite-gravity missions. Different models of the Late Pleistocene ice–ocean mass redistribution indicate secular geoid changes above 1 mm yr^{-1} over large parts of West Antarctica, with the amplitude depending on the timing of the deglaciation. Over East Antarctica, the signal of past ice mass changes is significantly reduced. Present-day mass imbalances result in a secular geoid rate, which is more localized as a consequence of the measurements, with amplitudes above ± 1 mm yr^{-1} over regions with large mass imbalances, locally exceeding 3–4 mm yr^{-1}. However, separating contributions of the last glacial cycles from present-day ice imbalances remains difficult, especially in view of the large uncertainties in the timing of the deglaciation in the LGM ice models. The spatial variability of the observed $\dot{g}$ may contain clues about the origin of the time-dependent geoid anomalies, with smaller-scale features more likely to be the result of present-day ice imbalances, and larger-scale features attributable to past ice volume changes.

Dependences upon different plausible mantle viscosity profiles are of secondary importance for model predictions. The predictions of the secular change of the geoid anomaly are at most affected by about 0.2 mm yr^{-1} by variations between different viscosity models. Hence, the principal uncertainty for the interpretation of the secular change of the geoid anomaly will arise from uncertainties in the past and present ice volume change.

ACKNOWLEDGMENTS

I would like to thank Philippe Huybrechts for his Antarctic Ice Sheet model, and Thomas James for the present-day Antarctic mass imbalance scenarios. John Wahr has provided the error estimates for the GRACE satellite-gravity mission. Constructive reviews from Bert Vermeersen and an anonymous referee have helped to improve the manuscript. The figures in this paper were drawn using the GMT graphics package (Wessel & Smith 1991).

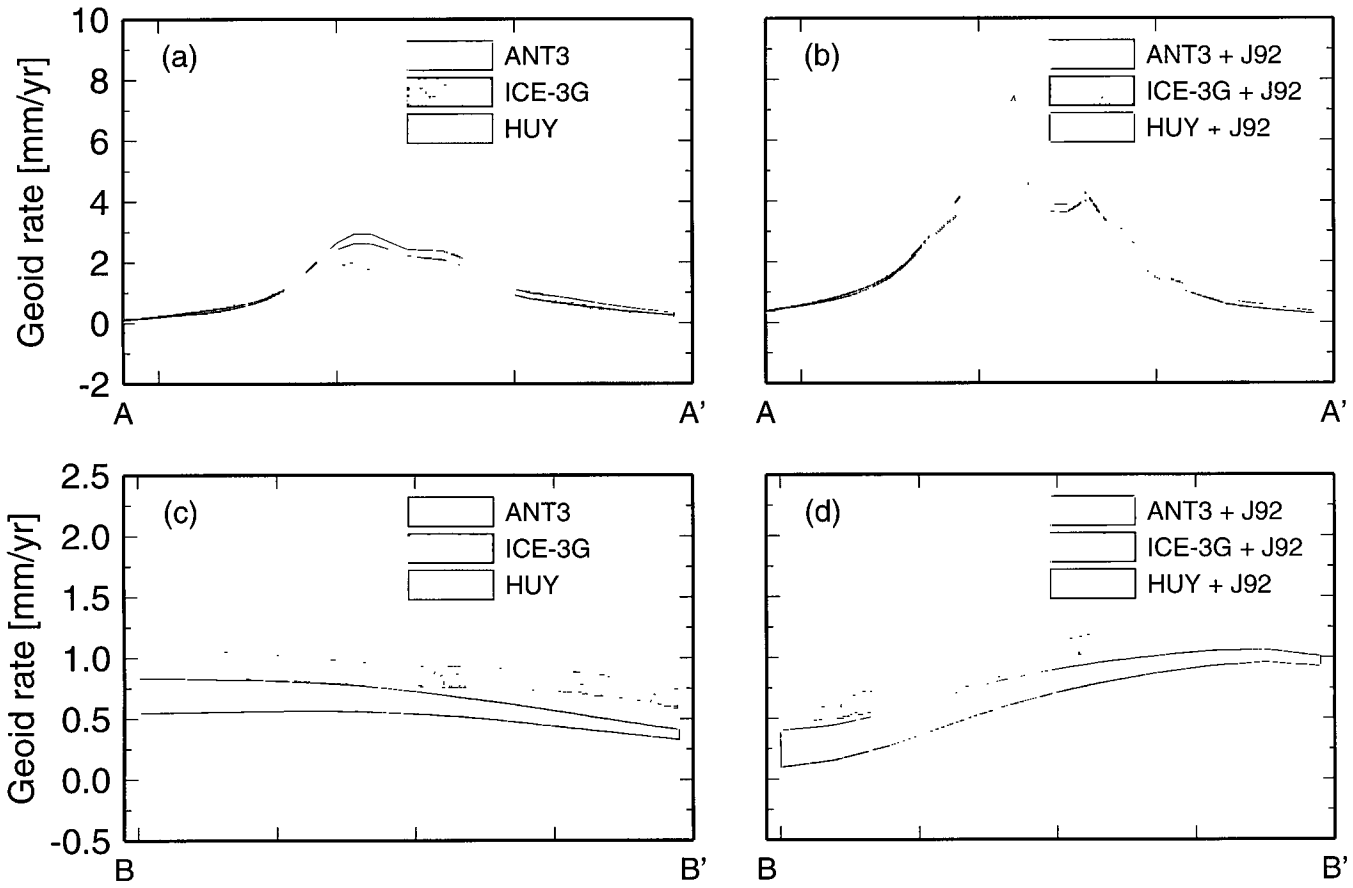

Figure 5. Range of predictions for secular variations in geoid anomaly (in mm yr^{-1}) along two profiles A–A′ (a and b) and B–B′ (c and d) shown in Fig. 2(d), based on the viscosity profiles shown in Fig. 1.

REFERENCES

Bentley, C.R. & Wahr, J.M., 1998. Satellite gravity and the mass balance of the Antarctic ice sheet, *J. Glaciol.*, **44,** 207–213.

Chappell, J. & Shackleton, N.J., 1986. Oxygen isotopes and sealevel, *Nature,* **324,** 137–140.

Denton, G.H. & Hughes, T.J., 1981. *The Last Great Ice Sheets,* John Wiley & Sons, New York.

Denton, G.H., Prentice, M.L. & Burckle, L.H., 1991. Cainozoic history of the Antartic ice sheet, in *Geology of Antarctica,* pp. 365–433, ed. Tingey, R.J., Oxford University Press, New York.

Drewry, D.J., 1982. *Antarctica: Glaciological and Geophysical Folio,* Scott Polar Research Institute, Cambridge.

Dziewonski, A.M. & Anderson, D.L., 1981. Preliminary reference Earth model, *Phys. Earth planet. Inter.,* **25,** 279–356.

Gornitz, V., Lebedeff, S. & Hansen, J., 1982. Global sea level trend in the past century, *Science,* **215,** 1611–1614.

Han, D. & Wahr, J., 1995. The viscoelastic relaxation of a realistically stratified Earth, and a further analysis of postglacial rebound, *Geophys. J. Int.,* **120,** 287–311.

Huybrechts, P., 1990. The Antarctic ice sheet during the last glacial-interglacial cycle: a three-dimensional experiment, *Ann. Glaciol.,* **14,** 115–119.

James, T.S. & Ivins, E.R., 1995. Present-day Antarctic ice mass changes and crustal motion, *Geophys. Res. Lett.,* **22,** 973–976.

James, T.S. & Ivins, E.R., 1997. Global geodetic signatures of the Antarctic ice sheet, *J. geophys. Res.* **102** (B1), 605–633.

James, T.S. & Ivins, E.R., 1998. Predictions of Antarctic crustal motions driven by present-day ice sheet evolution and by isostatic memory of the Last Glacial Maximum, *J. geophys. Res.,* **103,** 4993–5017.

Johnston, P. & Lambeck, K., 1999. Postglacial rebound and sea level contributions to changes in the geoid and the Earth's rotation axis, *Geophys. J. Int.,* **136,** 537–558.

Kaufmann, G. & Lambeck, K., 2000. Mantle dynamics, postglacial rebound and the radial viscosity profile, *Phys. Earth planet Inter.,* **121,** 303–327.

Kaufmann, G. & Lambeck, K., 2002. Glacial isostatic adjustment and the radial viscosity profile from inverse modeling, *J. Geophys. Res.,* accepted for publication.

Lambeck, K., 1993. Glacial rebound of the British Isles—II. A high-resolution, high-precision model, *Geophys. J. Int.,* **115,** 960–990.

Lambeck, K.,Smither, C. & Johnston, P., 1998a. Sea-level change, *Geophys. J. Int.,* **134,** 102–144.

Lambeck, K., Smither, C. & Ekman, M., 1998b. Tests of glacial rebound models for Fennoscandia based on instrumented sea- and lake-level records, *Geophys. J. Int.,* **135,** 375–387.

Milne, G.A. & Mitrovica, J.X., 1998. Postglacial sea level change on a rotating Earth, *Geophys. J. Int.,* **133,** 1–19.

Mitrovica, J.X. & Peltier, W.R., 1991. On postglacial geoid subsidence over the equatorial oceans, *J. geophys. Res.,* **96** (B12), 20 053–20 071.

Nakada, M. & Lambeck, K., 1988. The melting history of the late Pleistocene Antarctic ice sheet, *Nature,* **333,** 36–40.

Peltier, W.R. & Andrews, J.T., 1976. Glacial–isostatic adjustment—I. The forward problem, *Geophys. J. R. astr. Soc.*, **46,** 605–646.

Reigber, C., Bock, R., Förste, C., Grunwaldt, L., Jakowski, N., Lühr, H., Schwintzer, P. & Tilgner, C., 1996. CHAMP Phase B Executive Summary, *Technical Rept STR96/13*, GeoForschungsZentrum Potsdam.

Tushingham, A.M. & Peltier, W.R., 1991. Ice–3G: a new global model of late Pleistocene deglaciation based upon geophysical predictions of post-glacial relative sea level change, *J. geophys. Res.*, **96,** 4497–4523.

Wahr, J., Han, D. & Trupin, A., 1995. Predictions of vertical uplift caused by changing polar ice volumes on a viscoelastic Earth, *Geophys. Res. Lett.*, **22,** 977–980.

Wessel, P. & Smith, W.H.F., 1991. Free software helps map and display data, *EOS, Trans. Am. geophys. Un.*, **72,** 441–446.

Zwartz, D., Tregoning, P., Lambeck, K., Johnston, P. & Stone, J., 1999. Estimates of present-day glacial rebound in the Lambert Glacier region, Antarctica, *Geophys. Res. Lett.*, **26,** 1461–1464.